



Interpretation of multispectral satellite data as a tool for detecting archaeological artifacts (Navkur Plain and Karamleis Plain, Iraq)

Tomasz Pirowski¹ · Bartłomiej Szypuła² · Michał Marciak³

Received: 14 April 2022 / Accepted: 22 July 2022
© The Author(s) 2022

Abstract

Contemporary studies of geographical space, including archaeological research, incorporate multiple spatial digital data. Such data provide an opportunity to extend research to large areas, and to objectify studies on the basis of quantitative data thus obtained and gaining access to the hard-to-reach study area. Examples of such data are satellite images at various spatial resolutions and in a wide spectrum of electromagnetic radiation (visible, infrared, and microwave). The authors made an attempt to use satellite images to analyze the areas of probable location of the Battle of Gaugamela (the Navkur Plain and the Karamleis Plain in Iraq). The photointerpretation was performed, enhanced by the multivariate processing of the multispectral image. The aim of the work was indicating the most likely places where the camp and the battle were located based on the visual interpretation of an array of satellite data. The adopted methodology of precise allocation of interpretative values to remote sensing materials for every detected artifact provided an opportunity to accumulate an extensive amount of information. It also provided the basis for a synthetic analysis regarding the methods of image processing on the one hand and the dates of recording on the other. It turned out that the season in which the photos are recorded is very important—although the best data for analysis turned out to be the autumn data (38% of all recognized artifacts), the use of data from three seasons increased the total number of indicated artifacts by as much as about 50% (the so-called unique detections). In addition, advanced image processing (such as principal component analysis and decorrelation stretch) turned out to be important, as it increased the number of areal artifacts by 31% compared to the interpretation of only photos in natural (true) color composite and false color composite (with near-infrared). The conducted analyses have confirmed the usefulness of high-resolution satellite data for archaeological applications, and the detected and described anomalies visible in satellite images are excellent material for selecting sites for detailed field research.

Keywords Multispectral satellite data · Image processing · Gaugamela · Navkur Plain · Karamleis Plain

Introduction

This paper is part of ongoing research of multidisciplinary character involving the methods of ancient history, archaeology, Geographic Information Systems (GIS), and satellite remote sensing. The researchers' intention is to contribute to solving the long-standing enigma of the location of one of the most significant and famous battles of the ancient world—the Battle of Gaugamela. The Battle of Gaugamela was fought in 331 BCE between the Greek-Macedonian army under the command of Alexander the Great and the Persian army led by its king Darius III (Marsden 1964; Dąbrowa 1988). Alexander's victory at Gaugamela certainly changed history—it led to the collapse of the vast Persian kingdom (539–331 BCE) and the beginning of a new age

✉ Bartłomiej Szypuła
bartlomiej.szypula@us.edu.pl

¹ Department of Photogrammetry, Remote Sensing of Environment and Spatial Engineering, AGH University of Science and Technology, Al. Mickiewicza 30, 30-059 Kraków, Poland

² Institute of Earth Sciences, Faculty of Natural Sciences, University of Silesia in Katowice, Będzińska 60, 41-200 Sosnowiec, Poland

³ Institute of Jewish Studies, Faculty of History, Jagiellonian University in Kraków, Józefa 19, 31-056 Kraków, Poland

now widely known as the Hellenistic period (circa 331–30 BCE) (Austin 1981; Bugh 2006).

Notwithstanding the great importance of this battle, its precise location has been contested (Seibert 1972). Two main locations have been put forward over the course of the last two centuries of research—the Navkur Plain near Tell Gomel in Kurdish Iraq (Markwart 1905; Marsden 1964; Schachermeyr 1973; Fiey 1965; Reade and Anderson 2013) and the vicinity of modern Mosul in northern Iraq (Sushko 1936; Stein 1942; Badian 2000; Zouboulakis 2015, 2016). However, it should be stressed that the majority of modern scholars support the localization of the famous battle in the Navkur Plain. This identification can be argued on several premises: first, the continuity of local onomastics—the name Tell Gomel can be considered a remnant of the ancient name Gaugamela (Fales and Del Fabbro 2014: n. 6; Morandi Bonacossi and Iamoni 2015, 12, n. 8); second, the existence of a long-distance travel route between Nisibis and Arbela leading through the Navkur Plain in the times of Alexander the Great (Marciak et al. 2020); third, the appropriate topographic and geomorphological features in the Tell Gomel Plain (Marciak et al. 2022). At the same time, the identification in the Karamleis Plain features several serious deficiencies (Marciak et al. 2021a, b). First, its origin was deeply conditioned by the very limited regional experience of the earliest European explorers. The location of Tell Gomel was not yet known to the earliest European explorers, and Karamleis had the advantage of being located on the axis of contemporary travel between Mosul, Erbil, and Baghdad. Furthermore, the use of GIS recently revealed that this identification lacks some fundamental topographical and geomorphological features: visibility on the battlefield and a distinctive accumulation of sloped areas. In our present project, an attempt has been made to bring another aspect of the identification to the fore—namely, possible remains of military camps at the battlefield of Gaugamela, potentially discoverable with the use of satellite archaeology.

The hope that traces of the Macedonian camp could be discovered in the course of archaeological works expressed by Ritter (1840) a long time ago has not been realized so far. Nevertheless, we decided to consider the possibility, as it was recently implied by Reade and Anderson (2013), that such traces could be buried under the current surface and might be revealed with the application of modern technologies, especially remote sensing (as was the case with many Roman marching camps discovered in Europe, mainly in the UK, Germany, and South Moravia in Czechia (Roth 1999; Hanel 2007)); these have sometimes been acknowledged as successors to the Macedonian marching camps (Lévêque 1957; Champion 2009). Owing to the problematic character of the artifacts subject to the search (imprecise historical descriptions and lack of archaeological analogies), photo interpretation of satellite image data was selected as the

main research tool. The principles of photo interpretation, including the significance of direct (shape, color, and size) or indirect (e.g., shade) photo-interpretative qualities of features, as well as the utilization of false color composites, were discussed extensively by Jensen (2000) and Lillesand et al. (2015), among others.

Contemporary studies of geographical space, including archaeological research, incorporate multiple spatial digital data (satellite and aerial data, laser scanning, SAR, digital elevation models, and others) (see Linck et al. 2013; Stewart et al. 2016; Stewart 2017; Checa and Reche 2018; Evans and Mourad 2018; Peppas et al. 2018; Hadjimitsis et al. 2019; Kalayci et al. 2019; Luo et al. 2019; Blanco et al. 2020). Such data provide an opportunity to extend research to large areas, to acquire a bird's-eye view perspective and, most of all, to objectify studies on the basis of quantitative data thus obtained. The question of gaining access to the study area, especially hard-to-reach or no-entry areas (like in our case), is another essential aspect. Moreover, a large variety of Earth's satellite photos makes it possible to register information about the surface of areas with manifold spatial resolutions and with a wide spectrum of electromagnetic radiation (visible, infrared, and microwave). It is accompanied by a continuously growing availability of image data connected with a dynamically increasing number of registering platforms and resources with free archived data (USGS-NASA Landsat missions, ESA Sentinel-2, MODIS, SPOT, and many others), which are effectively applied to archaeological research (Ur 2006; Parcak 2009).

Considering the above, the authors of this article made an attempt to incorporate satellite images into the analysis of the areas indicated by historians and archaeologists as the most likely locations of the Battle of Gaugamela. The focus was on the northern location—the Navkur Plain—and the southern location—the Karamleis Plain (Fig. 1). Owing to lack of reference standards which would make way for automating the recognition process, photo interpretation, reinforced with multivariate processing of multispectral images, was adopted as the only legitimate and possible method at this stage. In accordance with the elementary principles of photo interpretation (the importance of direct and indirect photo-interpretative features), a search intended to identify the occurrence of sites (the so-called anomalies, artifacts) was conducted. Usually these surface features are either geometrical or have no justification with regard to the current land use (e.g., humidity and/or vegetation). A natural character of such places is certainly possible; however, there are chances they are of anthropogenic origin and, as such, testify to the existence of underground archaeological remains.

The ultimate goals of the research included:

1. Indicating the most likely places where the camp and/or the battle were located based on the visual interpreta-

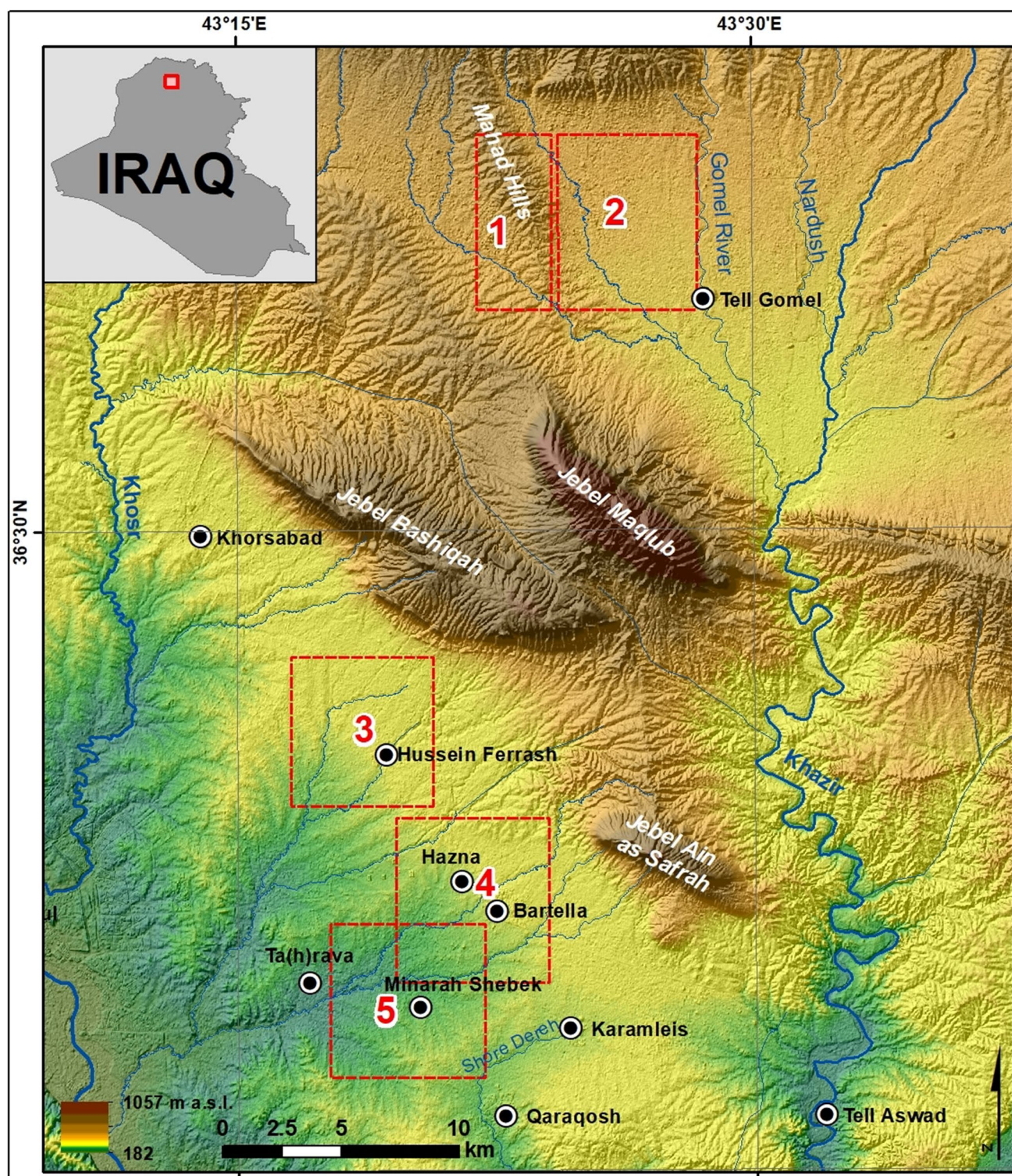


Fig. 1 Geographical context and study sites: 1, Mahad Hills (MH); 2, Tell Gomel Plain (TG); 3, Hussein Ferrash (HF); 4, Bartella-Khazna (BK); 5, Minarah Shebek (MS)

tion of an array of satellite data. Considering the limitations to free access to these areas in particular, such activities may provide practical benefits in terms of narrowing

the areas that would require field work and/or determining priority research areas.

2. Verifying the applicability of multispectral satellite imaging to this type of research. Such an analysis was

conducted on the hills of the Navkur Plain (Pirowski et al. 2021) and provided preliminary conclusions on how to structure an appropriate collection of image data. The main conclusion drawn from this research was the need for complimentary interpretative work on data registered in different seasons, both on the basis of standard color compositions from RGB + NIR bands and products derived from multivariate processing of multispectral bands. Vegetation indices proved to be less applicable. The analysis conducted in this article, which is an extension of previous studies of one area to the total of five, and the suggested new methodology of assessing the interpretative value of data provide a more extensive basis for drawing conclusions and justifying prior observations.

Study area

The study area is located in contemporary northern Iraq, with its center determined by the coordinates of 36°30' north latitude and 43°24' of east longitude (Fig. 1). It is situated between two major rivers: the Khosr in the west and the Khazir in the east. This area is the foreland of the Zagros Mountains, which stretch nearly latitudinally several dozen kilometers to the north. The highest elevations are located in the central part and they are made up of such hill chains as Jebel Maqlub (1057 m a.s.l.) and Jebel Bashiqa (661 m a.s.l.), as well as smaller ones: Mahad Hills (490 m a.s.l.) in the north and Jebel Ain as Safrah in the south (673 m a.s.l.). All of them create a natural watershed chain between the Khosr and Khazir Rivers. Elevation differences of the entire area amount to nearly 900 m (min 182 m a.s.l., max 1057 m a.s.l., and mean 347 m a.s.l.). It testifies to a great morphological diversity of the area of less than 2000 km². The climate of this area is determined by its intercontinental location and belongs to the tropical continental dry type, with a mean annual temperature of +21 °C. It is characterized by two distinct seasons: dry and hot summer (mean +32°) and cooler and more humid winter (mean +8°). Precipitation is low, averaging 380 mm per year, which leads to the occurrence of numerous intermittent rivers.

As the site of the battle has not been unambiguously determined, its location is still subject to discussion. It results from the condition of the preserved historical sources which, unfortunately, do not provide precise geographical and topographical information (Seibert 1972). Moreover, multiple significant accounts include contradictory information: for example, according to Arrian (Robson 1954) the battlefield of Gaugamela was situated 111 km away from the city of Arbela, while according to Curtius Rufus (Rolfe 1946) only about 14 km from the Great Zab River. Ultimately, over the last two centuries of research, several locations of ancient Gaugamela have been put forward:

Karamleis (Niebuhr 1776), Qaraqosh (Sushko 1936), Tell Aswad (Spiegel 1851), (a mound to the south of) Wardak (Schweiger-Lerchenfeld 1876)—currently referred to as the southern hypothesis—and Tell Gomel (Hoffmann 1880; Sachau 1883; Von Oppenheim 1900)—called the northern hypothesis. The above premises became the basis for conducting a detailed analysis of the areas potentially connected with the battle site. The authors marked 5 areas to be covered by the analysis: Mahad Hills and Tell Gomel Plain in the north and Hussein Ferrash, Bartella-Khazna, and Minarah Shebek in the south (Fig. 1). All these sites were suggested by previous scholars as possible alternative locations of the Macedonian military camps before the battle. The Mahad Hills were proposed as the location of the Macedonian final camp and the Tell Gomel plain as the actual battlefield by Marciak et al. (2021b). Hussein Ferrash and the vicinity of two nearby towns, Bartella and Khazna, were put forward by Sushko (1936) as the sites of the penultimate and ultimate camps of the Macedonian troops respectively, while Stein (1942) considered Minarah Shebek to have been the place of the Macedonian final camp.

Data

In the first stage, a relevant collection of satellite image data of very high resolution (0.5×0.5 m SVHR) was obtained for each investigated area (Bartella-Khazna, Minarah Shebek, and Hussein Ferrash in the Karamleis Plain, as well as Mahad Hills and Tell Gomel Plain in the Navkur Plain). The utilized satellite data included various time points from the period between 2013 and 2020 (Table 1). The selected data derived from two sensors: Pleiades and WorldView-2. Considering the above, the initial task was to standardize the materials in the way that would provide identical underlying satellite data from each of the five examined areas during the interpretation. The collection of basic data contained the total of 15 satellite image scenes—three images obtained for different seasons in each of the five locations (Table 1).

Previous research conducted in the Navkur Plain (Pirowski et al. 2021) indicated that the difference in spatial resolution between original multispectral images (2 m) and images of spatial resolution enhanced by the integration with a panchromatic image (up to 0.5 m) is crucial, especially for detecting linear features. On the other hand, the applied merge algorithm was of no relevance. Therefore, new materials involving the areas of Bartella-Khazna, Minarah Shebek, and Hussein Ferrash were acquired as MS + PAN integrated images of band spatial resolution artificially increased from 2 to 0.5 m. For the Navkur Plain region, for which WorldView-2 data (independently integrated with various methods) were available, merged data obtained with the

Table 1 Characteristics of satellite data used in the analyses

Satellite characteristics	Study site	Repository, data acquisition (Bands B, G, R, NIR—0.5 m) Orthophoto, WGS84/UTM EPSG: 32,638	Image processing to enhance the photointerpretation properties (for each area, at each registration date)
WorldView-2 © DigitalGlobe	The Navkur Plain (Mahad Hills)	ID10300100388F8C00 Summer/autumn: 28.09.2014	Color Composites True Color
Panchromatic band (PAN) spatial resolution: 0.5 m	The Navkur Plain (Tell Gomel Plain)	ID10300100388F8C00 Summer/autumn: 28.09.2014	Bands B-G-R (CC TC)
0.45–0.80 μm			Color Composites
Multispectral bands (MS) spatial resolution: 2 m			False Color
Coastal: 0.40–0.45			Bands G-B-NIR (FCC CIR)
Blue: 0.45–0.51			Color composites containing princi- pal components
Green: 0.51–0.58			PCA1-PCA2- PCA3 (CC PCA123)
Yellow: 0.58–0.62			Color composites containing princi- pal components
Green: 0.63–0.69			CC PCA2-PCA3- PCA4 (CC PCA234)
Red Edge: 0.70–0.75			Color composites with decorrela- tion stretch
NIR1: 0.77–0.90			(CC DS 123)
NIR2: 0.86–1.05			Color composites with decorrela- tion stretch
Multispectral bands after data fusion (merging HPF)			(CC DS 234)
(MS + PAN) spatial resolution: 0.5 m			Vegetation indices
Blue: 0.43–0.55 μm			Normalized Difference
Green: 0.50–0.62 μm			Vegetation Index (NDVI)
Red: 0.59–0.71 μm			Image after HPF filtration in a 3×3 kernel
NIR1: 0.74–0.94 μm			(HPF 3×3)
Pleiades 1A, 1B	The Navkur Plain (Mahad Hills)	DS_PHR1A_201304110806519 Spring: 11.04.2013	Image after HPF filtration in a 11×11 kernel
© CNES (2015—2020), Distribution Airbus DS		DS_PHR1B_201512120807314 Winter: 12.12.2015	(HPF 11×11)
Panchromatic band (PAN) spatial resolution: 0.5 m	The Navkur Plain (Tell Gomel Plain)	DS_PHR1A_201304110806519 Spring: 11.04.2013	
0.47–0.83 μm		DS_PHR1B_201512120807314	
Multispectral bands (MS) spatial resolution: 2 m		DS_PHR1B_201512240814454 Winter: 12.12 + 24.12.2015	
Blue: 0.43–0.55 μm			
Green: 0.50–0.62 μm			
Red: 0.59–0.71 μm			
NIR: 0.74–0.94 μm			
Multispectral bands after data fusion (merging)	The Karamleis Plain (Hussein Ferrash)	DS_PHR1B_201512190803436 Winter: 19.12.2015	
(MS + PAN)		DS_PHR1B_201604200806366 Spring: 20.04.2016	
Spatial resolution: 0.5 m		DS_PHR1A_201710070753028 Summer/autumn: 07.10.2017	
Blue: 0.43–0.55 μm			
Green: 0.50–0.62 μm			
Red: 0.59–0.71 μm			
NIR: 0.74–0.94 μm			
	The Karamleis Plain (Bartella- Khazna)	DS_PHR1A_201612300803176 Winter: 30.12.2016	
		DS_PHR1B_201905010800506 Spring: 01.05.2019	
		DS_PHR1B_201708270807474 Summer/autumn: 27.08.2017	
	The Karamleis Plain (Minarah Shebek)	DS_PHR1B_202001020807188 Winter: 02.01.2020	
		DS_PHR1B_201905150753084 Spring: 15.05.2019	
		DS_PHR1B_201708270807474 Summer/autumn: 27.08.2017	

high-pass filtering method HPF were selected for the analyses (Schowengerdt 1980; Chavez et al. 1991).

The works conducted in the Navkur Plain (Pirowski et al. 2021) revealed no increased interpretative usefulness

of atypical spectral ranges, which were provided by WV-2 (yellow band, RedEdge band, Near Infra Red NIR 2 s band). Information recorded in the bands typical of SVHR recording, i.e., RGB + NIR, proved to be of major importance.

These conclusions encouraged the authors to obtain data for the new research areas (the Karamleis Plain) from the Pleiades sensor, which has such a spectral profile, to serve as a sufficient supplementation of already available data for the northern location. At the same time, for the purpose of standardization of interpretative materials, only 4 out of WV-2 bands were used: RGB and NIR1.

In order to ensure the possibility of detecting diversified features, it was significant to provide data from different seasons. It gave an opportunity to highlight (depending on a season) the differences in local moisture of uncovered soils and their structural and textural features (winter, autumn), vegetation (spring, autumn), and the dissimilarities in drying out (autumn). Detailed descriptions of the applied data sets have been comprised in Table 1.

Methods

Detecting a group of surface and linear anomalies is more reliable and comprehensive if the underlying satellite material is diversified and consists of both classical color compositions and further processing. A complementary utilization of such data may verify questionable indications (e.g., the material originating from a particular season or properly processed by enhancing the content of the image can reveal unique features which make it possible to identify a given artifact).

Initially, for all the 15 satellite image scenes, two color compositions were prepared: True Color TC (Blue-Green-Red) in natural colors and Color Infra Red CIR (Green-Red + Near InfraRed) in fake colors. Then, each scene was subject to standardized transformation named principal component analysis (sPCA) (Lillesand et al. 2015; Richards 2013). The PCA transformation leads to obtaining a new uncorrelated set of images, the so-called principal components (PC). It provides an opportunity to develop new color compositions, different from those created on the basis of original spectral bands. In this case, a composition based on PC1, PC2, and PC3 components and PC2, PC3, and PC4 components was created. Subsequently, the PC123 and PC234 images were subject to principal components standardization and inverse transformation was conducted. This procedure is called decorrelation stretch and is usually performed on three selected spectral bands (DStretch) (Campbell 1996). It emphasizes the colors of areas which seem little differentiated in primary compositions. The DStretch procedure is particularly useful for composites containing highly correlated spectral bands characterized by low contrast and poor coloring (e.g., a composite in true colors, also CIR composite to a lesser extent). Owing to these activities, a new array of spectral bands and new images were acquired.

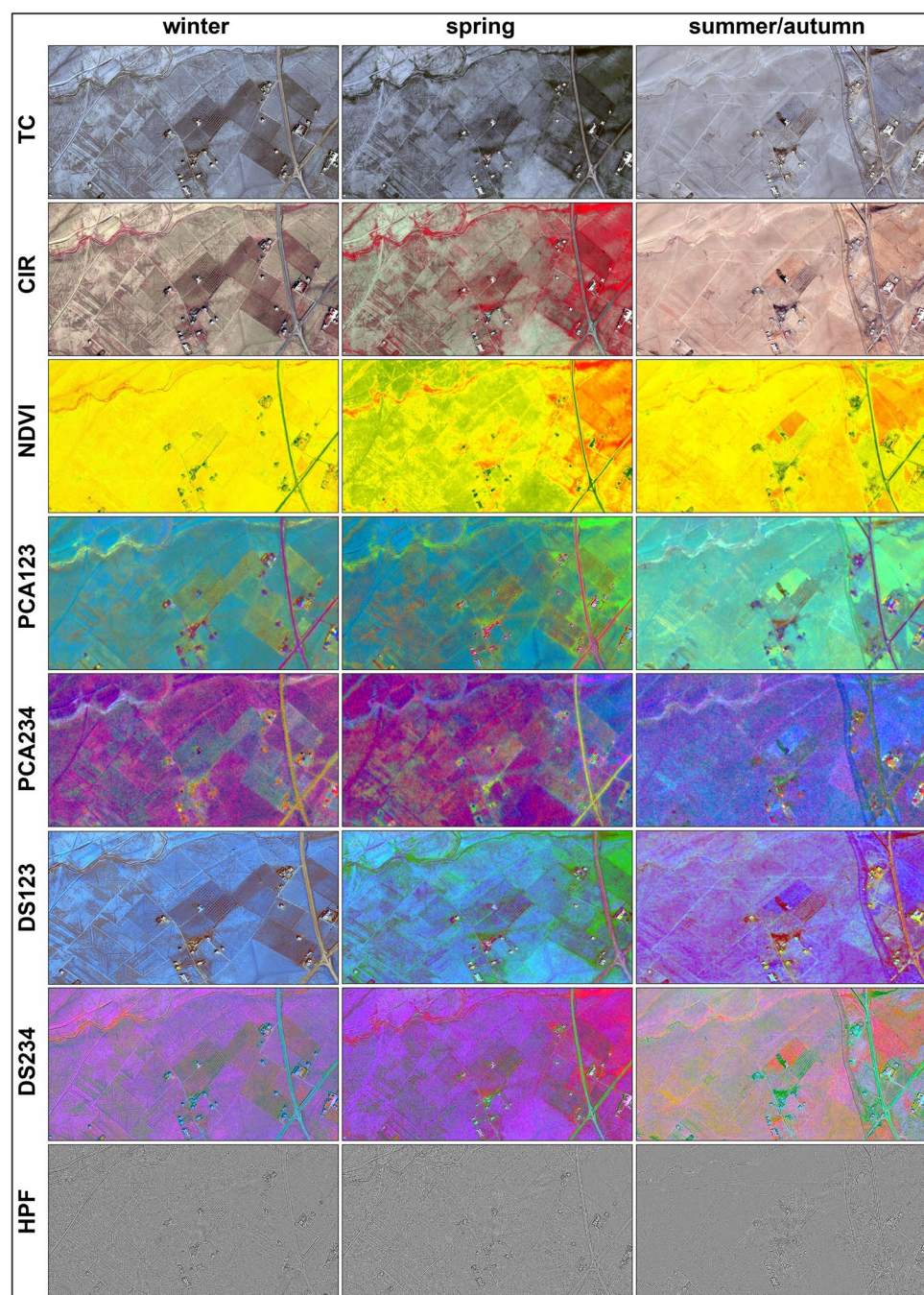
The next stage consisted in calculating the Normalized Difference Vegetation Index (NDVI) for all the 15 scenes (Agapiou et al. 2012; Kalayci et al. 2019). The NDVI is an indicator defining the quantitative share of vegetation (biomass) in a particular area and may highlight the features related to the local diversity of vegetation in a more efficient way than color compositions.

The final stage was the use of a high-pass filter (HPF), allowing the detection of edges. This highlights areas of tonal change in the image, running in any direction, and is used in archaeological interpretation (Lasaponara and Masini 2012; Sarris et al. 2013; Mondino et al. 2012). Since a grayscale image is used for filtering, a WorldView-2 panchromatic image was used for processing for the analysis area of The Navkur Plain (Mahad Hills and Tell Gomel Plain), for the autumn term. In the other cases, only Pleiades RGB and NIR images were available, after fusion with the panchromatic image (PAN). The PAN image was simulated by averaging the brightness from 4 channels, with a weighting of 0.5 introduced for the NIR channel (in the Pleiades, the PAN image only partially covers the NIR band). The option of using the first PCA component from the RGB + NIR channels was also tested, but the post-filtered image had less detail. After initial tests, it was considered useful to filter in a larger window, i.e., 11×11 (HPF11), apart from the base 3×3 filtering kernel (designation in the text: HPF3).

Consequently, 9 new images were drawn up on the basis of the 15 scenes of multispectral satellite images (see Table 1, last column). Therefore, the total of 135 images were subject to interpretation. An exemplary complete set of image data (27 images in total) for the Hussein Ferrash site in the form of a small fragment of the scene has been illustrated in Fig. 2.

The anticipated linear and surface anomalies (artifacts) in the context of the search for the Macedonian camp were the subject of detailed and multivariate characteristics in the earlier study (Pirowski et al. 2021). Field verification for the Navkur region did not bring about the expected results related to finding possible remains. It confirmed the concerns that possibly no remnants of former camps (a levelled bank or a shallower trench, etc.) have been preserved to the present day. Natural erosive processes, and anthropogenic activity and events occurring in this area throughout such an extensive period of time (over 2300 years) have caused that the camp boundaries—if they are successfully detected—may probably have linear outlines of a geometrical shape identifiable only from the air/satellite perspective and not ground-based observations. In such a case, in order to indicate its potential locations in a satellite image, the only trace can be the occurrence of an anomaly (artifact) in this area, which results from former ground disturbance or the existence of foreign elements in the soil. Depending on the

Fig. 2 An example of a set of image data for interpretation; a fragment of the Hussein Ferrash (HF) area of 1200 m×800 m



landform and coverage of the area, it may be reflected in multiple ways. Former facilities can manifest themselves in the contemporary topography through a specific distribution of vegetation (connected with the spheres of moisture) or even, in a broader context, through the development and layout of transportation or settlement networks. In fewer cases, it may be directly observed in the images (e.g., changes in the spectral response of the soil, which can be noticed in the areas not covered by vegetation). The contemporary fragmented character of the camp may be another impediment to the identification of its remains. Regardless of the assumed

shapes and area of the camp (30 ha), as well as the length of linear features (400 m), there might be no artifacts of such dimensions in the image. It is also possible that when the camp was established natural land features (the river system or ridge lines), which could have been its sides, were used. For that reason, the theoretically presupposed rectangular shape of the camp might not have ever been realized.

Table 2 provides a collection of expected major photo-interpretative features searched for in the created 135 color compositions and grayscale images, potentially relating to particular traces of the camp.

Table 2 Sought-after elements and related photointerpretation features anticipated in the satellite imagery (after Pirowski et al. (2021) changed)

1. Sought-after element 2. Character of element 3. Possible current state	Photointerpretation features, associations, indicators	Leading expected photo-interpretation feature in the CC TC, FCC, NDVI
1. Camp's earthen rampart about 1–2 m high and wide (palisade removed because it was portable), trench, adjacent, and parallel to the rampart of the camp about 1–2 m deep and wide	Direct features: On exposed soil, the occurrence of another spectral response (soil change) Texture change ("cutting" of existing textures on uncovered soil, dense vegetation)	Spectral Texture
2. Linear elements of unknown shape and course, limiting the area of the camp, each side from 0.4 to 1.5 km long. Possibility of adapting parts of the rampart and trench to the local terrain, including linear elements existing in this area (watercourses, paths)	Indirect features, associations: Other moisture of the former trench associated with the change in the soil structure (most often – more dryness than in the surroundings) Other vegetation/vegetation rate related to the violation of the original soil structure	Moisture Vegetation
3. Completely leveled rampart, silted up with natural processes and/ or a trench covered by human activity (agriculture, urbanization)	Geomorphological features (drainage network, dorsal network), the presence of paths, watercourses at the locations of the rampart/trench (provided that its layout was adapted to the existing terrain or the axis of the rampart/trench became a transportation route with time) A contrasting, spectral, or textural border extending over a longer section between different areas	Geomorphology Paths Watercourses Border
1. Area of the marching camp, part of the inner layout of the camp (for instance, the royal headquarters)	Direct features: The area inside the mapped contour of the camp rampart, with possible accompaniment or continuity through geomorphological elements of the terrain, such as paths or watercourses	Contour Spectral anomaly
2. An area between 30 and 235 ha, presumably square or rectangular; geometrized small-scale infrastructure of the camp. Geometrized small-scale infrastructure of the camp	Shape, size—small-scale residues related to the inner layout of the camp	Contour Texture anomaly
3. Agricultural activity, natural vegetation, local anomaly. Geometrized remains of small features	Indirect features: No contour, local anomaly characterized by a different spectral or textural response compared to the surrounding environment No contour, local anomaly characterized by varied spectral response/texture, partly different from the surrounding environment	Varied anomaly Varied anomaly

During the photo-interpretative analysis, the scale for assessing the value of single materials ranging from 0.0 (invisible) to 1.0 (the best material for detecting the polygon/line) was adopted. Intermediate values, i.e., 0.25, 0.5, and 0.75, which denoted partly applicable material, were also accepted. Having identified a feature, the adopted values were assigned to all the employed materials in a particular area on every single occasion (27 images = 27 assessments).

An exemplary scoring for one of the polygons is presented in Table 3. In this particular example, marking the boundaries of polygons was most efficient in the DS234

color composition and in the material recorded in spring (the most reliable, precise, and easily discernible). Regular compositions such as CC TC and FCC CIR, as well as NDVI (spring data), were also relatively applicable. Their values of 0.75 imply that the underlying material was more difficult to interpret or that the boundaries of a feature were not easily identifiable in its selected minor parts. The dropping values, e.g., those taken for the winter recording (0.5), are tantamount to the growing deterioration of the readability of images, which entails a less and less reliable identification of features (difficulties in their detection and/or an increasing

Table 3 An exemplary scoring for one of the analyzed polygons

Period	TC	CIR	NDVI	PCA123	PCA234	DS123	DS234	HPF 3	HPF 11
Winter (I)	0.50	0.50	0.00	0.50	0.00	0.50	0.00	0.00	0.25
Spring (II)	0.75	0.75	0.75	0.50	0.25	0.25	1.00	0.25	0.50
Autumn (IV)	0.00	0.00	0.25	0.75	0.25	0.00	0.25	0.00	0.00

share of layout fragments in features which are difficult to mark). The applied methodology of an individual assessment conducted for every detected feature was used for both lines and polygons in all the 5 study areas. It is an extension of the methodology suggested by Pirowski et al. (2021), where only the best readings involving a season (without the gradation of applicability) together with a major interpretative feature determining the detection were registered. In the solution adopted in this study, a comprehensive database was built for every artifact regarding the possibility of detection and including detailed information about the applicability of a particular image material.

In the first stage, the analysis was performed for every type of material in all the images “one by one” (e.g., all the 15 TC-BGR images for the 5 study areas were analyzed, then all the CIR images, etc.) In order to secure the impartiality of detecting artifacts in each subsequent underlying material (NDVI, PCA, DS, HPF, etc.), the analysis of images was conducted after a longer time limit, on data which were artificially rotated by 90, 180, or 270°, with no access to the information on the previously marked features. This stage made it possible to identify materials whose applicability for the detected artifacts amounted to 0.75–1.

In the second stage, the results (marked lines and polygons in various underlying images) were matched and their compatibility was verified. In the case of major discrepancies in their course, the numerical values of applicability were reduced for relevant image data. For example, when in three materials the course drawn for a linear feature was consistent, but in a certain fragment of another one a divergent/incorrect course compared to the previous three was observed or the feature was incomplete/shorter, such a case resulted in decreasing the applicability from 0.75/1 to a lower one, depending on the recognized degree of such a material deficiency. On the other hand, based on consistent interpretations from several materials, the ultimate outline of a surface area or the final course of a linear feature was determined.

In the third stage, it was verified whether the marked linear and surface features are modelled in the materials which had been considered to be of zero applicability in Stage I. Can they be detected anyway, for example, less credibly,

fragmentarily, or with conspicuous errors in the course of their layout? If yes, they were attributed the applicability of 0.25.

The analyses of multispectral satellite data were carried out in QGIS 3.10 (Open Source Geospatial Foundation Project 2020) software with plugin SCP (Semi Automatic Classification) and Idrisi Kilimanjaro (Clark Labs 2006). Additionally, the calculations of vector layers and the graphic work were conducted in ArcGIS (ESRI 2020) software.

Results and discussion

Quantity and spatial distribution of the identified features

The summary of data on the number and size of indicated locations regarding the study areas is presented in Table 4. The total of 131 features was detected: 45 polygons and 86 lines, which would require field examination. Assuming that the limit value is 30 ha, the condition was fulfilled by only 12 features, while subsequent 9 features met it conditionally (features with the area of 15–30 ha—the aforementioned uncertainties resulting from the possibility to detect the remains or part of the camp area exclusively). Additionally, the requirement of 400 m in length for a line was fulfilled by 80 out of 86 indicated features. Consequently, taking into account the size threshold for both surface and linear features, 92 features would call for field verification (12 surface and 80 linear ones). It may be easily noticed that mainly a small area of detected polygons contributes to the aggregate decrease in the number of features (merely 12 out of 45 features). By including partly preserved fragments of the former camp and lowering the limit to 15 ha, the total of 21 polygons could be covered by the study.

Should we investigate the overall number of marked features with respect to the division into examined areas, we will notice that the largest numbers of detected features were recorded for the Tell Gomel and Hussein Ferrash areas (over 30). It mainly results from a big amount of linear features.

Figures 3, 4, 5, 6, 7 and 8 present a special layout of marked linear and polygon features for each study area.

Table 4 Tabulation of the detected features for all study sites

Study site	Number of area objects				Number of line objects			
	All	≥30 ha	15–30 ha	Mean area	All	≥400 m	<400 m	Mean length
1. Mahad Hills (MH)	7	-	2	8 ha	16	13	3	691 m
2. Tell Gomel (TG)	10	4	3	27 ha	24	23	1	1066 m
3. Hussein Ferrash (HF)	5	-	-	7 ha	32	30	2	1001 m
4. Bartella-Khazna (BK)	10	4	1	23 ha	6	6	-	857 m
5. Minarah Shebek (MS)	13	4	3	33 ha	8	8	-	1229 m
Total:	45	12	9	19.6 ha	86	80	6	968.8 m

These are potential archaeological research sites, the purpose of which is to detect the remains of a military camp from fourth century BCE. No characteristic layout or interrelated co-occurrence of the discovered features (e.g., a polygon feature that would be surrounded/bordered with linear features resembling a geometrical shape) can be discerned. The most polygons were detected in the area of Minarah Shebek (Fig. 7), although it needs to be emphasized that some of them overlap. For each of the three areas (Tell Gomel, Bartella-Khazna, Minarah Shebek), 4 polygons measuring ± 30 ha were marked, while in the remaining two areas (Mahad Hills, Hussein Ferrash) the number of identified polygons was smaller and their average size was merely 7–8 ha (Table 4). In total, in all the five areas, only 12 polygons met the requirement of

reaching the size of 30 ha, which accounts for about one-fourth of all designated polygons.

The situation looks different in the case of lines: most of them were designated in the area of Hussein Ferrash (Fig. 5) and almost all of them exceed the length of 400 m, with the mean length of 1 km. Generally, as many as 93% of all identified lines meet the condition of length, while the average length of all the lines amounts to around 970 m (Table 4).

Considering the number of features detected in the images exclusively, the priority of field study should be given to the area of Hussein Ferrash (37 features), then Tell Gomel (34) and Mahad Hills (23), and finally Minarah Shebek (21) and Bartella-Khazna (16). It should however be noted that some polygons clearly mark the extent of lower towns around tells (see Fig. 5), and not boundaries of a military enclosure. Additionally, many linear features can be tentatively

Fig. 3 All line and polygon features distinguished on Mahad Hills study site (background image: DS234 autumn)

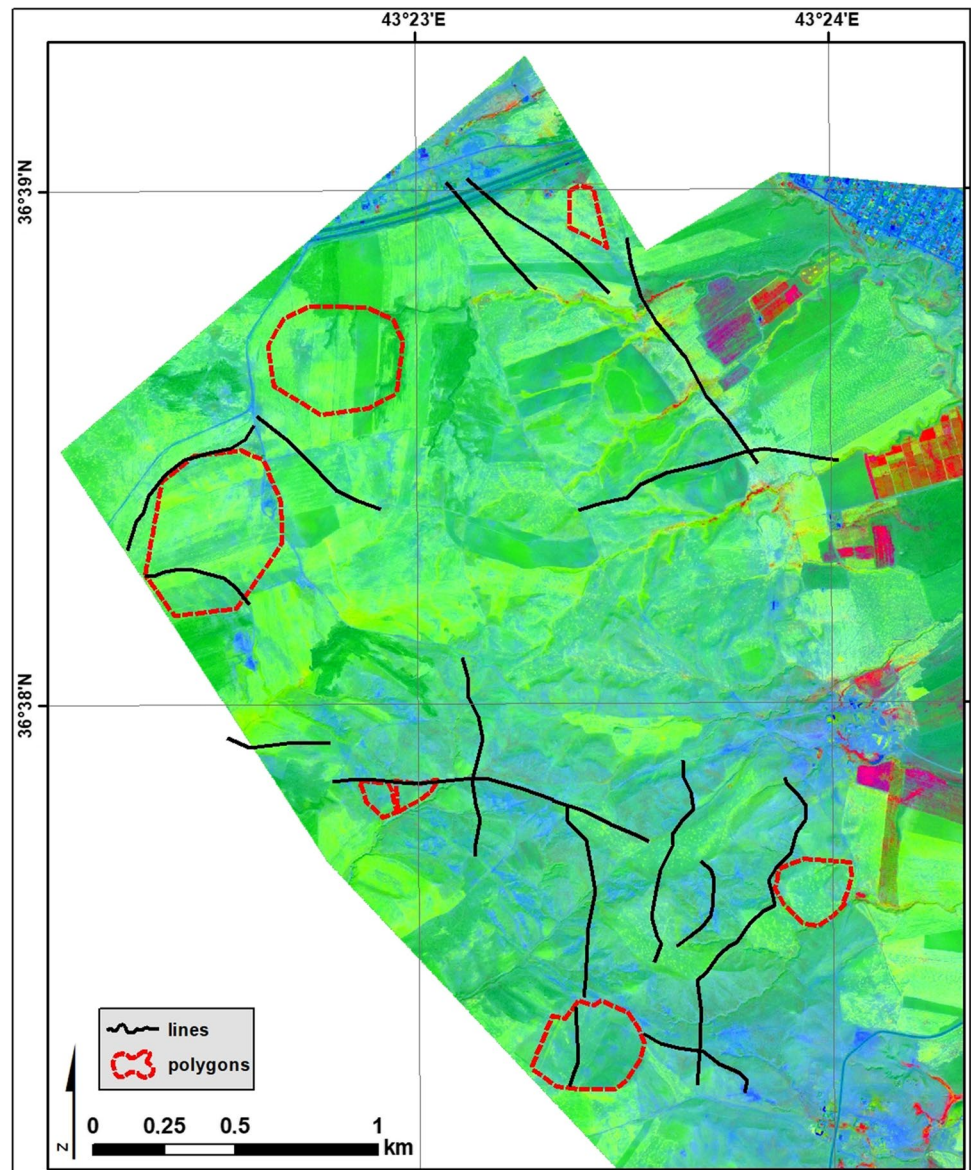
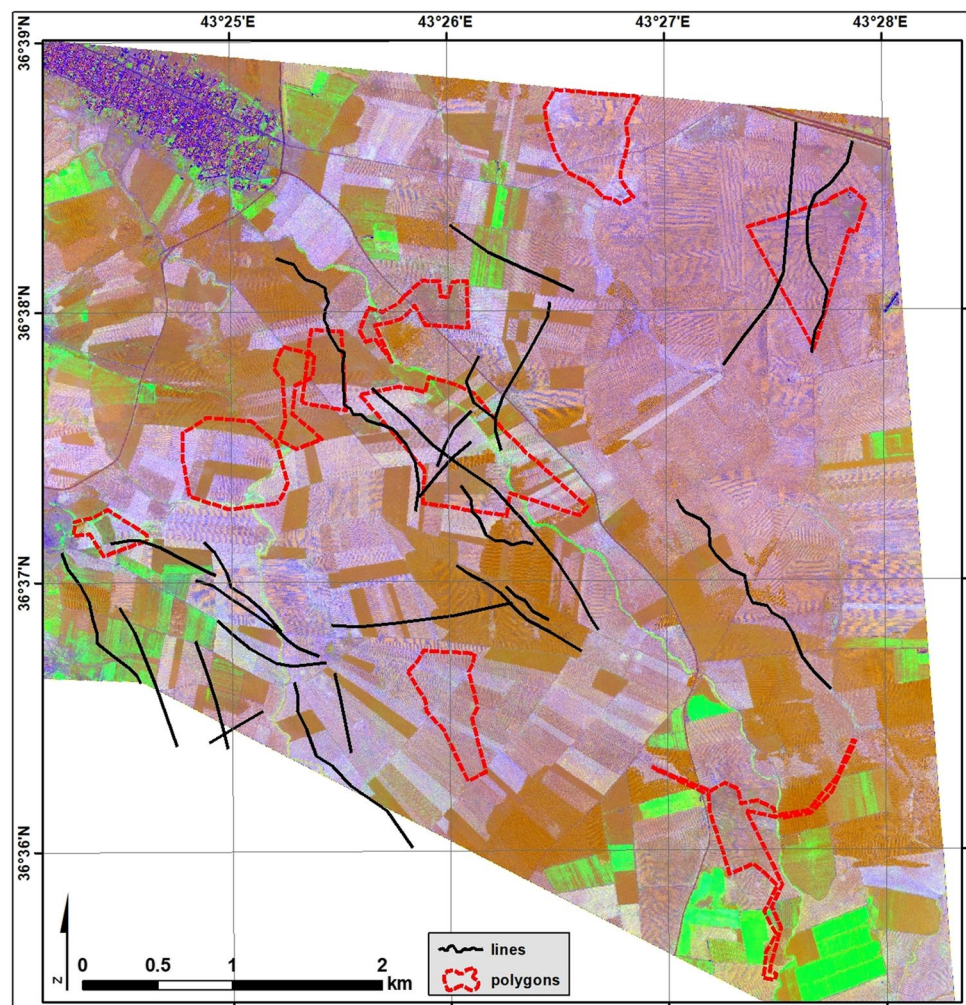


Fig. 4 All line and polygon features distinguished on the Tell Gomel study site (background image: PCA123 autumn)



identified as hollow ways, which are broad and shallow linear depressions in the landscape thought to be formed by the continuous passage of human and animal traffic (Ur 2003), and again not as the boundaries of a military structure.

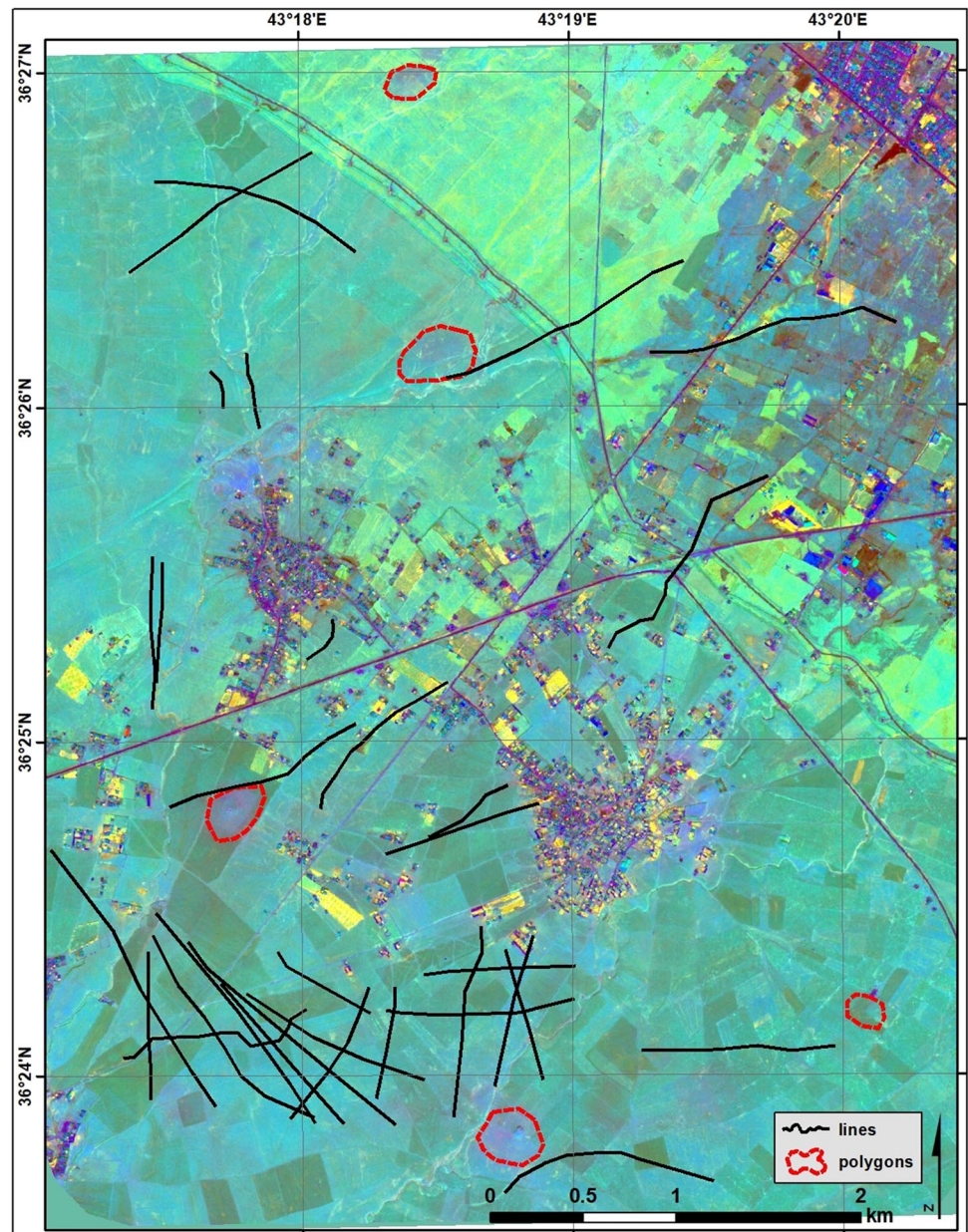
Interpretative value of remote sensing materials

The evaluation of the actual applicability of remote sensing materials can only be performed following a field verification. However, it may be assumed that featuring artifacts themselves—and, consequently, the opportunity to detect them more easily and geometrize them in particular remote sensing data and the products obtained from their processing—can be the basis for ranking image data. Such an approach was adopted in this work considering the fact that the very possibility of identifying surface anomalies, which is frequently difficult or even impossible to capture in the case of in situ work, leads to increasing the efficiency of field work (by indicating the possible locations of the searched historical traces). The total number of “photo interpretative points,” which contain the number of detections and the

information on how easy it was to designate them and how reliable these markings are, was considered equivalent to this applicability.

The interpretative analysis began with determining the degree of detectability of particular features expressed through a points system. Table 5 shows the amount of all detected features together with the average number of interpretative points per one feature (the quotient of interpretative points and the number of features). This parameter provides the information on the difficulty in detecting features—the lower the value, the more difficult the feature identification (i.e., feasible only in a limited amount of image data). The values varied considerably, depending on the study area and the type of features. On average, one detected feature had 4.9 photo-interpretative points; however, it was more complicated to detect polygons (the average of 3.7 points) than linear features (the average of 5.5) (Table 5). The highest mean point value for the detected lines amounted to 8.9 pts/feature (Mahad Hills), and 7.2 pts/feature for polygons (Hussein Ferrash). It confirms great sharpness of features searched for in the study, which are currently visible in

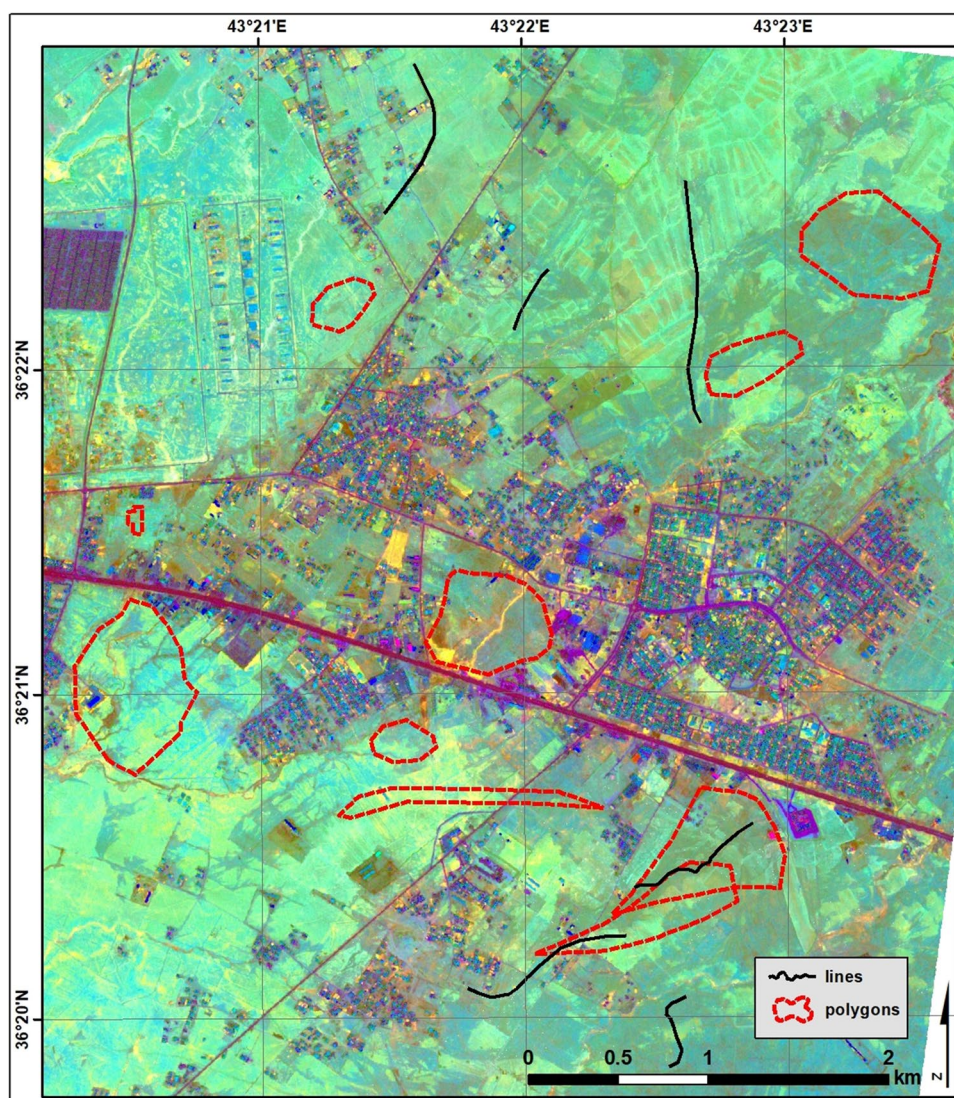
Fig. 5 All line and polygon features distinguished on the Hussein Ferrash study site (background image: PCA123 autumn)



numerous image data. On the other hand, the lowest values for lines (4.3 pts/feature) were obtained in Tell Gomel and for polygons (1.9 pts/feature) in the area of Minarah Shebek. These low numbers indicate that line objects occur twice less frequently here than in the area with the highest scoring, while polygons are nearly four times less common. All in all, the highest values were obtained for Mahad Hills, which may be accounted for by the fact that in the hills a number of borders of the artifacts subject to the study could be marked along natural, geomorphological elements of the landscape (ridges, watercourses), well-visible in the majority of the employed image materials. The lowest values, on the other hand, were recorded for Bartella-Khazna and Minarah Shebek (the average of 3.2–3.4 pts).

Table 5 also comprises the total number of points for the identified features (polygons, lines) divided into the employed image data for every study site. In all the areas, the amount of points awarded to linear objects is much higher, which results from the simple fact that nearly twice as many lines as polygons were detected. Only for the area of Bartella-Khazna is the number of points for both types of features similar. As far as image data with the highest amount of detected features are concerned, for lines these were CIR and TC data, which scored 41% of all points. In the case of polygons, the points were almost evenly distributed in all the data. NDVI and HPF data, which obtained the fewest points (and, consequently, were

Fig. 6 All line and polygon features distinguished on the Bartella-Khazna study site (background image: PCA123 autumn)



characterized by the lowest detectability of the sought-after features), were the only exception.

Determining the significance of recording the area in different seasons was another investigated element. Table 6 presents the total number of points awarded during the interpretation of image data, including the information on the type of data and the season of data acquisition. No prevailing season can be observed for polygon features. On the other hand, autumn proved to be the best season for detecting lines in the materials. It can also be noticed in the overall scores—autumn, as the period following plants vegetation, is conducive to the most effective identification of features visible topography.

As far as image data are concerned, the highest scores were obtained for FCC CIR (128.75 pts) and CC TC (118.25 pts), that is, classically applied color compositions. On the other hand, the NDVI turned out to be the least useful material (38 pts) and images after HPF filtration (9 pts + 25.25

pts). The remaining image data scored from 71.25 pts (DS123) to 92 pts (PCA123), but if analyzed jointly (as PCA transformation products), their total amount reached 318.25 pts. Therefore, it may be claimed, that if this additional image processing had not been applied, a smaller number of artifacts would have been detected (it is also confirmed by a detailed “unique feature detection” analysis, see in Table 7).

The final performed activity was the analysis of “unique feature detection,” which was supposed to check how many features (polygons and lines) were found in only one kind of image data (i.e., TC, CIR, NDVI, PCA123, PCA234, DS123, DS234) or grouped data (composites from TC and CIR, NDVI bands, composites based on PCA, HPF3 + HPF11) during the interpretation. Table 7 depicts this analysis for every study site. The following table reveals that 16% of all detected polygons are present in the image data of one type exclusively (e.g., PCA234). However, if we apply data composites, the number increases remarkably up to 40%

Fig. 7 All line and polygon features distinguished on the Minarah Shebek study site (background image: PCA123 autumn)

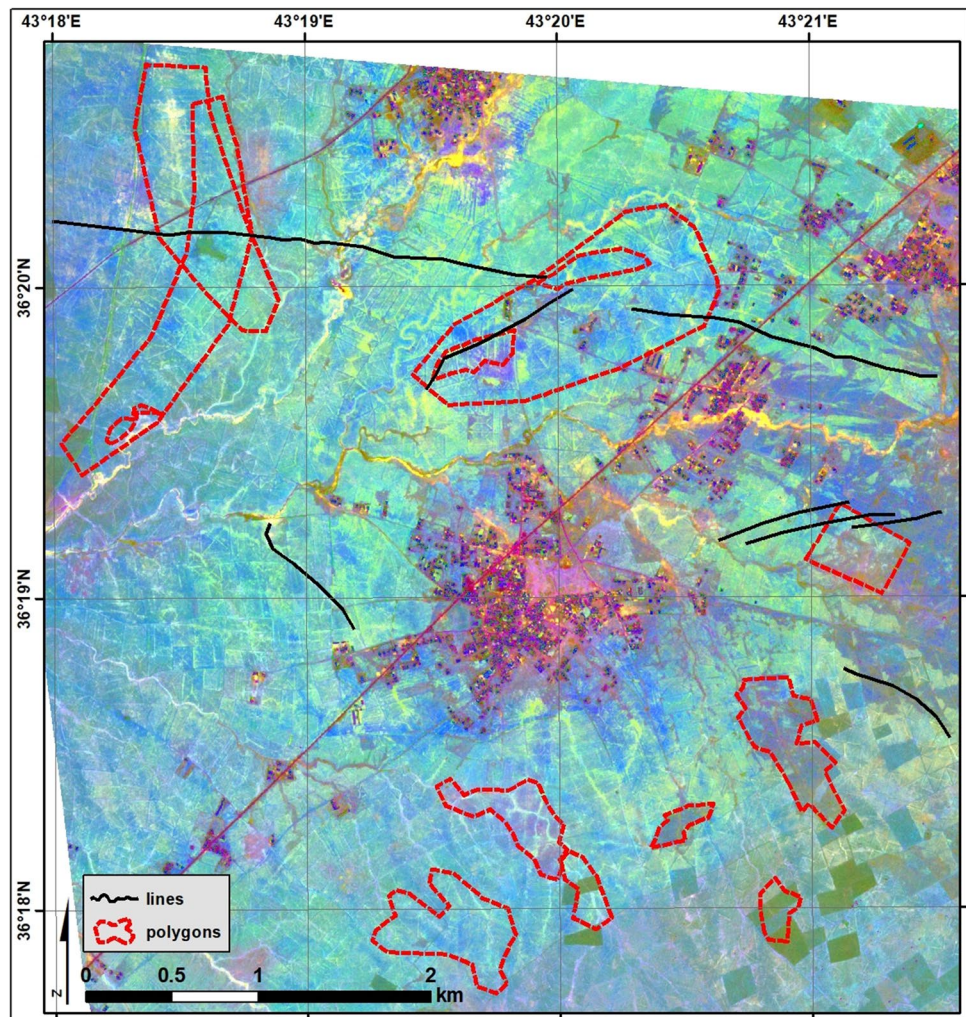


(Table 7). On the other hand, for linear features, the total amount of unique feature detection is considerably lower and ranges from 1 to 7%. Therefore, it may be stated that the PCA image material (CC PCA123, CC PCA234, DS123, DS234) actually increases the quantity of polygon and line features that are searched for. However, one should be aware that working solely on PCA composites would be insufficient and unreliable. Finally, it must be remarked that NDVI and HPF images were the only material where no unique features were observed. Consequently, employing NDVI and HPF should be considered of secondary importance, applicable only to support identification.

Additionally, Table 8 shows unique feature detections related to the season of image data acquisition. Numerical statistics of unique artifact detection reveal that around half of the detected features were noticed in the data from a particular season and were not visible in the others (56% for surface features, 47% for linear features). The aggregated data indicate the most features for autumn (68%), then for winter (20%) and the fewest for spring (12%).

Summary and conclusions

The adopted methodology of precise allocation of interpretative values to remote sensing materials for every detected artifact provided an opportunity to accumulate an extensive amount of information. It also provided the basis for a synthetic analysis regarding the methods of image processing on the one hand and the dates of recording on the other. The assessment of the applicability of the materials prepared for photo interpretation led to the following conclusions:

1. The significance of recording the site in various seasons is very high—the application of data derived from three seasons increased the number of designated locations by around 50% (the so-called unique detections). If it is necessary to conduct works in merely one dataset, it is recommended to employ autumn data (the most interpretative point values were awarded to the autumn data—38% of all). However, the scores for the remaining data, i.e., from winter and spring, are on a very similar level of 30–31%. Owing to high numbers of unique detections, working on

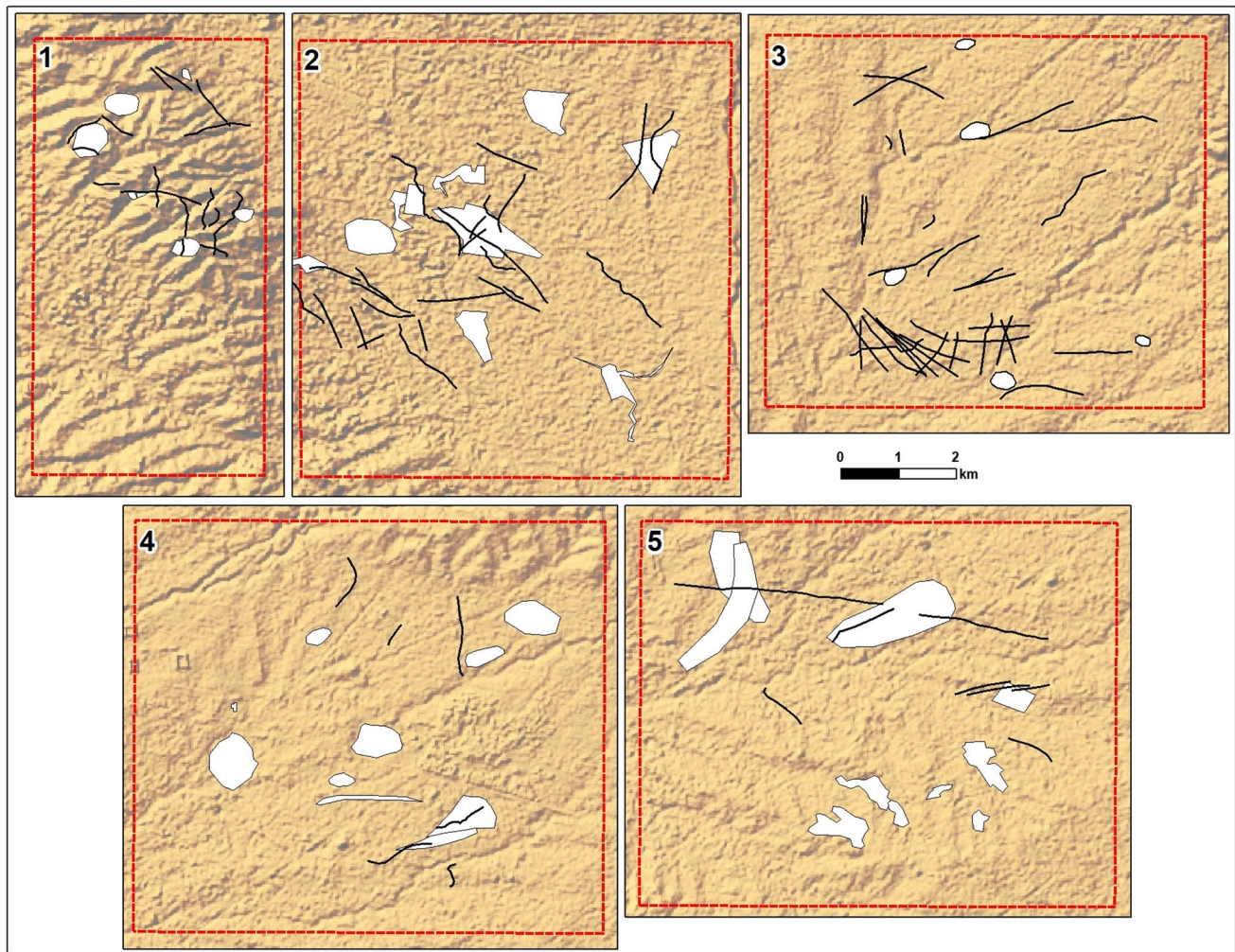


Fig. 8 All identified line and polygon features (study sites numbering in accordance with Fig. 1)

data from one acquisition period leads to the decrease in detection by around 30–38% (Fig. 9).

2. The importance of image processing is considerable. The work on color compositions from PCA and decorrelation stretch provided a greater amount of new locations (the so-called unique detections) than CC TC and FCC CIR themselves—31% more for surface features and 5% more for linear ones (the weighted average of 13.7%). No unique feature detection was obtained with the application of NDVI data. Having differentiated data available in numerous cases provides additional reliability of detection and facilitates marking the boundaries of features.

Owing to the new methodology, based on the obtained results, the impact of data acquisition from different seasons can be estimated more precisely—to be twice as significant as additional image processing from one date of recording (increase/decrease of detections: $\sim 30\text{--}37\%$ to $14.5\% > 2$) (Fig. 10).

3. Surprisingly low usefulness was noted for NDVI and HPF methods. It seems that the searching and delineation of artifacts based on image features (boundaries, texture, spectral features) that vary and change even within a single object limits the usefulness of an analysis based only on biomass intensity (as is the case with NDVI) or on object boundaries (as is the case with HPF). Perhaps the complementary use of spectral indices other than NDVI (including soil) would improve results in this group of data. On the other hand, for methods based on edge detection, it seems that an additional problem is the relatively large dimensions of the artifacts sought, often of a fuzzy nature. This is clearly visible for the reported very low suitability of HPF for polygons. Better results were obtained for linear objects, but it should be remembered that even they are often wider objects than the edges in the images, and therefore difficult to detect by filtering. This problem was partly solved using a larger filtering window, allowing for correctly mapping

Table 5 Tabulation of the sum of the scores during interpreting according to the image data

Features	Number of features (mean points per feature)	Image data and total points									Total number of points
		TC	CIR	NDVI	PCA123	PCA234	DS123	DS234	HPF3	HPF11	
Mahad Hills (MH)											
Polygons	7 (7.3)	8.5	8.75	1.5	5.75	8.25	3.75	8	2	4.5	51.0
Lines	16 (8.9)	27.5	29	7.5	16	17.75	13.5	15.5	5	10	141.75
Total	23 (8.4)	36	37.75	9	21.75	26	17.25	23.5	7	14.5	192.75
Tell Gomel (TG)											
Polygons	10 (3.1)	4.5	6.25	0.5	5.25	2.25	4.5	7.5	0	0.25	31.0
Lines	24 (4.3)	15.25	22	8.75	17.25	8.25	11	17	0	2.25	101.75
Total	34 (3.9)	19.75	28.25	9.25	22.5	10.5	15.5	24.5	0	2.5	131.75
Hussein Ferrash (HF)											
Polygons	5 (7.2)	4.5	4.5	4.75	5.5	4.75	5.5	6.25	0	0.5	36.25
Lines	32 (4.8)	33	33.75	12	18.5	16.5	22.5	13	0.25	4	153.5
Total	37 (5.1)	37.5	38.25	16.75	24	21.25	28	19.25	0.25	4.5	190
Bartella-Khazna (BK)											
Polygons	10 (2.4)	3.25	4.75	0.25	5.25	5.5	2.5	3	0	0	24.5
Lines	6 (5.0)	5.5	6.25	2	6.75	4.25	2	1.75	0.75	0.75	30.0
Total	16 (3.4)	8.75	11	2.25	12	9.75	4.5	4.75	0.75	0.75	54.5
Minarah Shebek (MS)											
Polygons	13 (1.9)	6.5	3.5	0	5.75	5	2	1.75	0	0.25	24.75
Lines	8 (5.4)	9.75	10	0.75	6	3.5	4	5.25	1	2.75	43.00
Total	21 (3.2)	16.25	13.5	0.75	11.75	8.5	6	7	1	3	67.75
All study sites in total:											
Polygons	45 (3.7)	27.25	27.75	7	27.5	25.75	18.25	26.5	2	5.5	167.5
Lines	86 (5.5)	91	101	31	64.5	50.25	53	52.5	7	19.75	470.0
Total	131 (4.9)	118.25	128.75	38	92	76	71.25	79	9	25.25	637.5

Table 6 Tabulation of the sum of the scores during interpreting according to the season of the image data acquisition

Features	Season	TC	CIR	NDVI	PCA123	PCA234	DS123	DS234	HPF3	HPF11	Total
Polygons	Winter	11.75	8.50	2.25	7.00	11.50	5.75	8.75	0.50	1.75	57.75
	Spring	6.50	10.00	3.25	8.50	6.25	4.75	9.75	0.75	2.25	52.00
	Autumn	9.00	9.25	1.50	12.00	8.00	7.75	8.00	0.75	1.50	57.75
Lines	Winter	28.75	29.50	5.75	17.00	17.75	16.25	13.25	2.50	6.25	137.00
	Spring	22.00	29.75	13.50	27.50	13.00	13.75	18.75	2.25	8.25	148.75
	Autumn	40.25	41.75	11.75	20.00	19.50	23.00	20.50	2.25	5.25	184.25
Total	Winter	40.50	38.00	8.00	24.00	29.25	22.00	22.00	3.00	8.00	194.75
	Spring	28.50	39.75	16.75	36.00	19.25	18.50	28.50	3.00	10.50	200.75
	Autumn	49.25	51.00	13.25	32.00	27.50	30.75	28.50	3.00	6.75	242.00

of larger structures by eliminating small-scale structures (higher HPF11 scores than HPF3). The NDVI and HPF in comparison with the CC and PCA/DS should be considered supporting data. The usefulness of the HPF method would certainly be greater for detailed work and for the analysis of the boundaries of small-scale objects.

4. The conducted analyses proved the applicability of high-resolution satellite data in detecting local artifacts

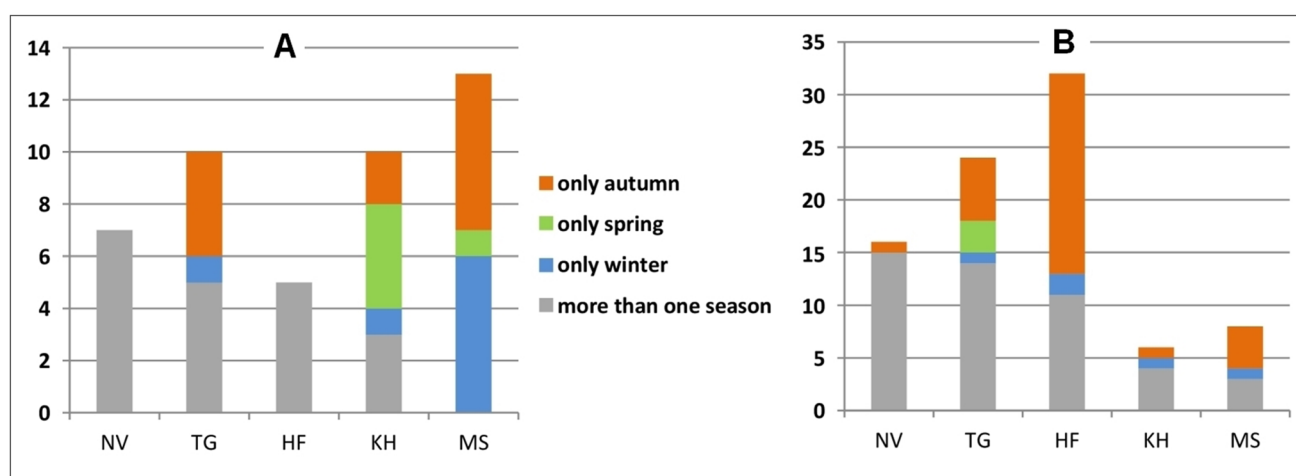
covered by vegetation and human activity and, consequently, difficult to identify in landscape during surface fieldwork. Generalization of data recorded from space ceiling is, undoubtedly, the factor which facilitates marking such features, both surface and linear ones. Generalization does not mean withdrawing from detailed imaging of the Earth surface, but the ability to include in an analysis and combine diverse information, volatility of the nature of artifacts in

Table 7 Unique feature detections related to the image data used

Study site	Unique/all features	TC	CIR	NDVI	PCA123	PCA234	DS123	DS234	HPF3	HPF11	% of all features
Polygon features											
MH	0/7	0	0	0	0	0	0	0	0	0	0%
TG	0/10	0	0	0	0	0	0	0	0	0	0%
HF	0/5	0	0	0	0	0	0	0	0	0	0%
BK	2/10	0	0	0	1	1	0	0	0	0	20%
MS	5/13	2	0	0	0	3	0	0	0	0	38%
Total	7/45	2	0	0	1	4	0	0	0	0	16%
MH	2/7	0		0	2				0		29%
TG	2/10	0		0	2				0		20%
HF	0/5	0		0	0				0		0%
BK	4/10	1		0	3				0		40%
MS	10/13	3		0	7				0		77%
Total	18/45	4		0	14				0		40%
Line features											
MH	0/16	0	0	0	0	0	0	0	0	0	0%
TG	0/24	0	0	0	0	0	0	0	0	0	0%
HF	0/32	0	0	0	0	0	0	0	0	0	0%
BK	0/6	0	0	0	0	0	0	0	0	0	0%
MS	1/8	0	0	0	1	0	0	0	0	0	12%
Total	1/86	0	0	0	1	0	0	0	0	0	1%
MH	0/16	0		0	0				0		0%
TG	1/24	0		0	1				0		4%
HF	3/32	2		0	1				0		9%
BK	1/6	0		0	1				0		17%
MS	1/8	0		0	1				0		13%
Total	6/86	2		0	4				0		7%

Table 8 Unique feature detections related to the season of the image data acquisition

Study site	Unique/all features	Winter	Spring	Autumn	% of all features
Polygon features					
MH	0/7	0	0	0	0%
TG	6/10	1	0	5	60%
HF	0/5	0	0	0	0%
BK	6/10	1	4	1	60%
MS	13/13	6	1	6	100%
Total	25/45	8	5	12	56%
Line features					
MH	1/16	0	0	1	6%
TG	11/24	1	3	7	46%
HF	21/32	2	0	19	66%
BK	2/6	1	0	1	33%
MS	5/8	1	0	4	62%
Total	40/86	5	3	32	47%
Polygon features + line features					
Total	65/131	13	8	42	50%
% of all features		20%	12%	68%	

**Fig. 9** Number of detected features resulting from using data for a specific season for polygons (A) and lines (B)

space, the interconnections between features and their environment, and the opportunity to determine their functions. All these aspects can be relatively easily studied both in the local (high-scale) and regional (low-scale) contexts.

Undeniably, the detected and described anomalies which are visible in the satellite images are merely introductory indications to conduct thorough fieldwork. They should be

considered a tool which provides an opportunity to reduce field research to areas of potentially highest chances for discovering the siting of the camp. Moreover, the possibility to carry out small-scale work on images gives the unquestionable advantage over fieldwork, which is usually performed within a short period of time, in a particular season, and in limited spatial coverage.

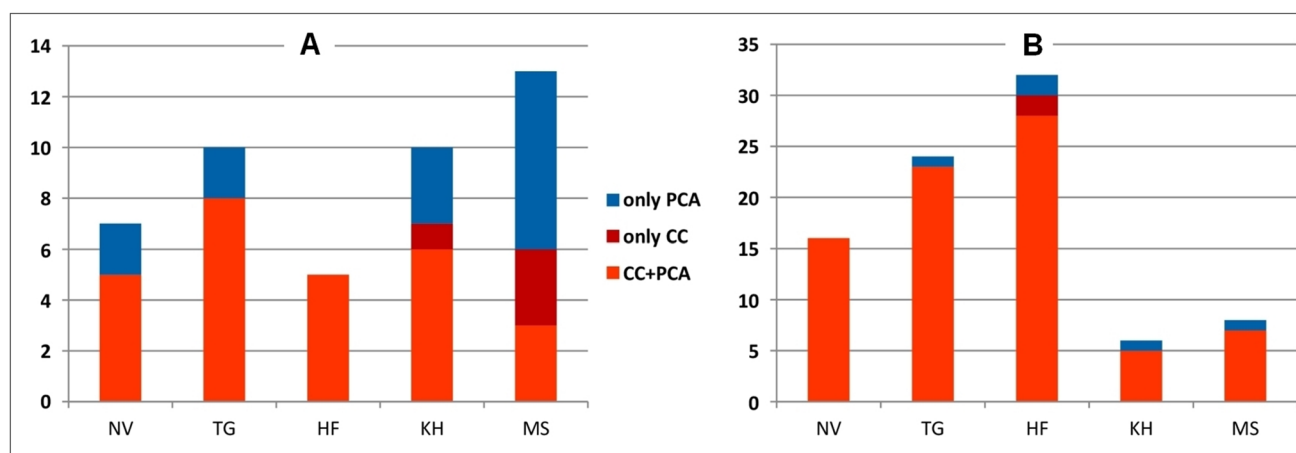


Fig. 10 Number of detected features resulting from using additional imaging processing for polygons (A) and lines (B)

Acknowledgements This paper presents a selected aspect of research conducted within the project entitled “Location of the Battle of Gaugamela in the Light of Multidisciplinary Research” (no. 2017/26/M/HS3/00750), which is financed by the National Science Centre in Poland. The project is affiliated at Jagiellonian University in Poland and is conducted in cooperation with the Land of Nineveh Archaeological Project of the University of Udine (Prof. Daniele Morandi Bonacossi).

Author contributions All the authors contributed to the study conception and design. Material preparation, and data collection and analysis were performed by TP. The first draft of the manuscript was written by TP and MM. All the figures were prepared by BS. Writing, modification, and synthetic summary of data analysis, review, and final paper editing were done by BS. All the authors commented on previous versions of the manuscript. All the authors read and approved the final manuscript.

Data availability Not applicable.

Code availability Not applicable.

Declarations

Conflict of interest The authors declare no competing interests.

Open Access This article is licensed under a Creative Commons Attribution 4.0 International License, which permits use, sharing, adaptation, distribution and reproduction in any medium or format, as long as you give appropriate credit to the original author(s) and the source, provide a link to the Creative Commons licence, and indicate if changes were made. The images or other third party material in this article are included in the article's Creative Commons licence, unless indicated otherwise in a credit line to the material. If material is not included in the article's Creative Commons licence and your intended use is not permitted by statutory regulation or exceeds the permitted use, you will need to obtain permission directly from the copyright holder. To view a copy of this licence, visit <http://creativecommons.org/licenses/by/4.0/>.

References

- Agapiou A, Hadjimitsis DG, Alexakis DD (2012) Evaluation of broadband and narrowband vegetation indices for the identification of archaeological crop marks. *Remote Sensing* 4:3892–3919. <https://doi.org/10.3390/rs4123892>
- Austin MM (1981) *The Hellenistic World from Alexander to the Roman conquest: a selection of ancient sources in translation*. Cambridge University Press, Cambridge
- Badian E (2000) Gaugamela. *Enc Iran* 10:332–333
- Blanco AM, Sánchez JG, Costa-García JM, Fonte J, González-Álvarez D, García VV (2020) Following the Roman Army between the Southern Foothills of the Cantabrian Mountains and the Northern Plains of Castile and León (North of Spain): archaeological applications of remote sensing and geospatial tools. *Geosciences* 10(12):485. <https://doi.org/10.3390/geosciences10120485>
- Bugh GR (ed) (2006) *The Cambridge companion to the Hellenistic World*. Cambridge University Press, Cambridge
- Campbell NA (1996) The decorrelation stretch transformation. *Int J Remote Sens* 17:1939–1949. <https://doi.org/10.1080/01431169608948749>
- Cartledge P (2005) *Alexander the Great. The Hunt for a New Past*. McMillan, London
- Champion J (2009) *Pyrrhus of Epirus*. Barnsley
- Chavez PS, Anderson JA, Side SC (1991) Comparison of three different methods to merge multiresolution and multispectral data: Landsat TM and SPOT Panchromatic. *Photogramm Eng Remote Sens* 57:295–303
- Checa AM, Reche TM (2018) COSMO SkyMed X-Band SAR application - combined with thermal and RGB images - in the archaeological landscape of Roman Mellaria (Fuente Obejuna-Córdoba, Spain). *Archaeol Prospect* 25:301–314. <https://doi.org/10.1002/arp.1709>
- Clark Labs (2006) *IDRISI Kilimanjaro* (v. 15.0). Clark University, Worcester
- Dąbrowa E (1988) *Gaugamela 331 p.n.e.* Warszawa
- ESRI (Environmental Systems Research Institute) (2020) *ArcGIS Desktop: Release 10.8.1.*, Redlands, CA

- Evans L, Mourad AL (2018) DStretch® and Egyptian tomb paintings: a case study from Beni Hassan. *J Archaeol Sci Rep* 18:78–84. <https://doi.org/10.1016/j.jasrep.2018.01.011>
- Fales FM, Del Fabbro R (2014) Back to Sennacherib's Aqueduct at Jerwan: a reassessment of the textual evidence. *Iraq* 76:65–98
- Fiey JM (1965) *Assyrie chrétienne. Contribution à l'étude de l'histoire et de la géographie ecclésiastiques et monastiques du nord de l'Iraq*. Beirut
- Hadjimitsis DG, Themistocleous K, Cuca B, Agapiou A, Lysandrou V, Lasaponara R, Masini N, Schreier G (eds.) (2019) *Remote sensing for archaeology and cultural landscapes*. Springer Remote Sensing Photogrammetry. <https://doi.org/10.1007/978-3-030-10979-0>
- Hanel N (2007) Military camps, Canabae, and Vici: the archaeological evidence, in P.A. Erdkamp (ed.), *Companion to the Roman Army*, Oxford, 395–416
- Heckel W, Yardley JC (2005) *Alexander the Great. Historical Sources in Translation*; Blackwell Publishing, Malden
- Hoffmann G (1880) *Auszüge aus Syrischen Akten Persischer Märtyrer*. Brockhaus, Leipzig
- James S (2015) Of colossal camps and a new Roman battlefield: remote sensing, archival archaeology and the “conflict landscape” of Dura-Europos, Syria. In: Breeze DJ et al. (ed) *Understanding Roman frontiers: a celebration for Professor Bill Hanson*, pp. 328–345
- Jensen JR (2000) *Remote sensing of the environment: an earth resource perspective*. Prentice Hall, Upper Saddle River
- Kalayci T, Lasaponara R, Wainwright J, Masini N (2019) Multispectral contrast of archaeological features: a quantitative evaluation. *Remote Sensing* 11:913. <https://doi.org/10.3390/rs11080913>
- Lasaponara R, Masini N (2012) Image enhancement, feature extraction and geospatial analysis in an archaeological perspective. In: Lasaponara R, Masini N (eds) *Satellite remote sensing. Remote Sensing and Digital Image Processing*, vol 16. Springer, Dordrecht. https://doi.org/10.1007/978-90-481-8801-7_2
- Lévéque P (1957) *Pyrrhos*, Paris
- Lillesand T, Kiefer RW, Chipman J (2015) *Remote sensing and image interpretation*. Wiley, New York
- Linck R, Busche T, Buckreuss S, Fassbinder JWE, Seren S (2013) Possibilities of archaeological prospection by high-resolution X-band satellite radar - a case study from Syria. *Archaeol Prospect* 20:97–108. <https://doi.org/10.1002/arp.1444>
- Luo L, Wang X, Guo H, Lasaponara R, Zong X, Masini N, Wang G, Shi P, Khatteli H, Chen F, Tariq S, Shao J, Bachagha N, Yang R, Yao Y (2019) Airborne and spaceborne remote sensing for archaeological and cultural heritage applications: a review of the century (1907–2017). *Remote Sens Environ* 232:111280. <https://doi.org/10.1016/j.rse.2019.111280>
- Marciak M, Głogowski P, Szypuła B, Pirowski T (2022) Gaugamela in the Plains of Nineveh? The southern location of the Battle of Gaugamela reconsidered. *Anabasis. Studia Classica et Orientalia* (forthcoming)
- Marciak M, Sobiech M, Pirowski T (2020) Alexander the Great's route to Gaugamela and Arbela. *Klio* 102:536–559
- Marciak M, Szypuła B, Sobiech M, Pirowski T (2021a) The Battle of Gaugamela and the question of visibility on the battlefield. *Iraq* 83:87–103. <https://doi.org/10.1017/irq.2021.11>
- Marciak M, Wójcikowski R, Morandi Bonacossi D, Sobiech M (2021b) The Battle of Gaugamela in the Navkur Plain in the context of the Macedonian and Persian art of warfare. *Stud Iran* 50:7–68
- Markwart J (1905) *Untersuchungen zur Geschichte von Eran*. Göttingen
- Marsden EW (1964) *The campaign of Gaugamela*. Liverpool
- Mondino BE, Perotti L, Piras M (2012) High resolution satellite images for archaeological applications: the Karima case study (Nubia region, Sudan). *European Journal of Remote Sensing* 45(1):243–259. <https://doi.org/10.5721/EuJRS20124522>
- MorandiBonacossi D, Iamoni M (2015) Landscape and settlement in the Eastern Upper Iraqi Tigris and Navkur Plains: The Land of Nineveh Archaeological Project, Seasons 2012–2013. *Iraq* 77:9–39
- Niebuhr C (1776) *Carsten Niebuhrs Reisebeschreibung nach Arabien und Andern Umliegenden Ländern*; (Band 2); N. Müller, Kopenhagen
- Open Source Geospatial Foundation Project (2020) QGIS (Geographic Information System v. 3.10.5). QGIS Development Team. Retrieved from: <http://qgis.osgeo.org>
- Parcak SH (2009) *Satellite remote sensing for archaeology*. Routledge, London, p 320
- Peppas MV, Mills JP, Fieber KD, Haynes I, Turner S, Turner A, Douglas M, Bryan PG (2018) Archaeological feature detection from archive aerial photography with a SfM-Mvs and image enhancement pipeline. In: *Proceedings of the International Archives of the Photogrammetry, Remote Sensing and Spatial Information Sciences, ISPRS TC II Mid-term Symposium “Towards Photogrammetry 2020”*, Riva del Garda, Italy, 4–7 June 2018; Volume XLII-2
- Pirowski T, Marciak M, Sobiech M (2021) Potentialities and limitations of research on VHRS data: Alexander the Great's military camp at Gaugamela on the Navkur Plain in Kurdish Iraq as a test case. *Remote Sensing* 13:904. <https://doi.org/10.3390/rs13050904>
- Reade JE, Anderson JR (2013) Gunduk, Khanes, Gaugamela, Gali Zardak – notes on Navkur and nearby rock-cut sculptures in Kurdistan. *Zeitschrift Für Assyriologie* 103(1):69–123. <https://doi.org/10.1515/za-2013-0008>
- Richards JA (2013) *Remote sensing digital image analysis. An Introduction*. Springer, Berlin
- Ritter C (1840) *Die Erdkunde im Verhältniß zur Natur und zur Geschichte des Menschen oder allgemeine, vergleichende Geographie*, T. 9. Berlin
- Robson EI (1954) *Arrian: With an English Translation E.I. Robson*, Vol. I, Books I–IV, the Loeb Classical Library. Cambridge, London
- Rolfe JC (1946) *Quintus Curtius With an English Translation J.C. Rolfe*, Vol. I, Books I–V, the Loeb Classical Library. Cambridge, London
- Roth J (1999) *The logistics of the Roman army at war (264 BC - AD 235)*. Leiden, Boston
- Sachau E (1883) *Reise in Syrien und Mesopotamien*. Brockhaus, Leipzig
- Sarris A, Papadopoulos N, Agapiou A, Salvi MC, Hadjimitsis DG, Parkinson WA, Yerkes RW, Gyucha A, Duffy PR (2013) Integration of geophysical surveys, ground hyperspectral measurements, aerial and satellite imagery for archaeological prospection of prehistoric sites: the case study of Vésztó-Mágor Tell, Hungary. *J Archaeol Sci* 40:1454–1470. <https://doi.org/10.1016/j.jas.2012.11.001>
- Schachermeyr F (1973) *Alexander der Grosse: Das Problem seiner Persönlichkeit und seines Wirkens*. Verlag der Österreichischen Akademie der Wissenschaften, Wien
- Schowengerdt RA (1980) Reconstruction of multispatial, multispectral image data using spatial frequency content. *Photogramm Eng Remote Sens* 46:1325–1344
- Schweiger-Lerchenfeld A (1876) *Ingenieur Josef Černík's Technische Studien-Expedition Durch Die Gebiete Des Euphrat Und Tigris Nebst. Ein-Und Ausgangs-Routen Durch Nord-Syrien*, 2. H. Justus Perthes, Gotha
- Seibert J (1972) *Alexander der Grosse*. Darmstadt
- Spiegel F (1851) *Die Alexandersage bei den Orientalen*. Verlag von Wilhelm Engelmann, Leipzig
- Stein A (1942) Notes on Alexander's Crossing of the Tigris and the Battle of Arbela. *Geogr J* 100:155–164
- Stewart C (2017) Detection of archaeological residues in vegetated areas using satellite synthetic aperture radar. *Remote Sensing* 9:118. <https://doi.org/10.3390/rs9020118>

- Stewart C, Montanaro R, Sala M, Riccardi P (2016) Feature extraction in the north Sinai Desert using spaceborne synthetic aperture radar: potential archaeological applications. *Remote Sensing* 8:825. <https://doi.org/10.3390/rs8100825>
- Sushko S (1936) Gaugamela. The Modern Qaraqosh. The Ukrainian academy of sciences of America, Chicago
- Ur JA (2006) Google Earth and Archaeology. The SAA Archaeological Record 6:35–38. Available at: <https://tinyurl.com/yczc2321>
- Von Oppenheim M (1900) Vom Mittelmeer zum Persischen Golf durch den Haurän, die Syrische Wüste und Mesopotamien. D. Reimer, Berlin
- Zambrini A (2007) The historians of Alexander the Great. In: A companion to Greek and Roman historiography. In: Marincola J (ed). Blackwell, Malden, pp. 210–220
- Zouboulakis K (2015) The topography of the Battle of Gaugamela: contributing to an old controversy. *Pharos* 21(2):31–62. <https://doi.org/10.2143/PHA21.2.3206294>
- Zouboulakis K (2016) Carrying the glory of the Great Battle. The Gaugamela battlefield: ancient sources, modern views and topographical problems. In: Kopanias K, McGinnis J (eds) The archaeology of the Kurdistan region of Iraq and adjacent regions. Oxford, pp. 437–455

Publisher's note Springer Nature remains neutral with regard to jurisdictional claims in published maps and institutional affiliations.